How to cite: *Angew. Chem. Int. Ed.* **2023**, *62*, e202310937
doi.org/10.1002/anie.202310937

Energy Storage Materials | Hot Paper

Poly(benzimidazobenzophenanthroline)-Ladder-Type Two-Dimensional Conjugated Covalent Organic Framework for Fast Proton Storage**

Mingchao Wang[+], Gang Wang[+], Chandrasekhar Naisa[+], Yubin Fu, Sai Manoj Gali, Silvia Paasch, Mao Wang, Haiko Wittkaemper, Christian Papp, Eike Brunner, Shengqiang Zhou, David Beljonne, Hans-Peter Steinrück, Renhao Dong,* and Xinliang Feng**

Abstract: Electrochemical proton storage plays an essential role in designing next-generation high-rate energy storage devices, e.g., aqueous batteries. Two-dimensional conjugated covalent organic frameworks (2D *c*-COFs) are promising electrode materials, but their competitive proton and metal-ion insertion mechanisms remain elusive, and proton storage in COFs is rarely explored. Here, we report a perinone-based poly(benzimidazobenzophenanthroline) (BBL)-ladder-type 2D *c*-COF for fast proton storage in both a mild aqueous Zn-ion electrolyte and strong acid. We unveil that the discharged C–O^- groups exhibit largely reduced basicity due to the considerable π-delocalization in perinone, thus affording the 2D *c*-COF a unique affinity for protons with fast kinetics. As a consequence, the 2D c-COF electrode presents an outstanding rate capability of up to 200 A g^{-1} (over 2500 C), surpassing the state-of-the-art conjugated polymers, COFs, and metal–organic frameworks. Our work reports the first example of pure proton storage among COFs and highlights the great potential of BBL-ladder-type 2D conjugated polymers in future energy devices.

Introduction

Electrochemical proton (H^+) storage plays an essential role in rechargeable aqueous batteries, for example, aqueous metal-ion (e.g. Zn^{2+}, Al^{3+}) batteries[1,2] and proton batteries,[3,4] which are intriguing next-generation energy storage devices benefiting from the intrinsic safety, low cost and high ionic conductivity of the aqueous electrolytes.[5,6] In

[*] Dr. M. C. Wang,[+] Dr. G. Wang,[+] Dr. C. Naisa,[+] Dr. Y. Fu, Dr. S. Paasch, Prof. E. Brunner, Prof. R. Dong, Prof. X. Feng
Center for Advancing Electronics Dresden (cfaed) and Faculty of Chemistry and Food Chemistry, Technische Universität Dresden
Mommsenstrasse 4, 01062 Dresden (Germany)
E-mail: xinliang.feng@tu-dresden.de

Dr. G. Wang[+]
Key Laboratory of Advanced Fuel Cells and Electrolyzers Technology of Zhejiang Province, Ningbo Institute of Materials Technology and Engineering, Chinese Academy of Sciences,
Ningbo 315201 (China)
E-mail: gang.wang@nimte.ac.cn

Dr. G. Wang[+]
University of Chinese Academy of Sciences
Beijing 100049 (China)

Dr. C. Naisa,[+] Dr. Y. Fu, Prof. X. Feng
Max Planck Institute of Microstructure Physics
Weinberg 2, 06120 Halle (Germany)

Dr. S. M. Gali, Dr. D. Beljonne
Laboratory for Chemistry of Novel Materials
University of Mons
Place du Parc 20, 7000 Mons (Belgium)

Dr. M. Wang, Dr. S. Zhou
Institute of Ion Beam Physics and Materials Research, Helmholtz-Zentrum Dresden-Rossendorf
01328 Dresden (Germany)

Dr. M. Wang
Laboratory of Micro-Nano Optics, College of Physics and Electronic Engineering, Sichuan Normal University
Chengdu 610101 (China)

H. Wittkaemper, Dr. C. Papp, Prof. H.-P. Steinrück
Institute of Physical Chemistry II, Friedrich-Alexander-Universität Erlangen-Nürnberg
Egerlandstr. 3, 91058 Erlangen (Germany)

Dr. C. Papp
Physical Chemistry, Freie Universität Berlin
Arnimallee 22, 14195 Berlin (Germany)

Prof. R. Dong
Key Laboratory of Colloid and Interface Chemistry of the Ministry of Education, School of Chemistry and Chemical Engineering,
Shandong University
250100 Jinan (China)
E-mail: renhaodong@sdu.edu.cn

[+] These authors contributed equally to this work.

[**] A previous version of this manuscript has been deposited on a preprint server (https://doi.org/10.26434/chemrxiv-2022-5kdvx).

conventional metal-ion batteries, metal ions, as the only charge carriers, suffer from slow diffusion kinetics, resulting in poor rate performance and long charging periods of devices;[7] while in aqueous metal-ion batteries, protons (H^+) with small ionic radii and minimum relative atomic mass could participate in the electrochemical energy storage process along with metal ions. Due to the ultrahigh mobility of H^+ in water via a Grotthuss mechanism,[8] the device performance of aqueous batteries can be largely elevated. Very recently, a Zn^{2+}/H^+ co-storage in framework cathodes has contributed to a much superior rate capability[9] over those adopting a mere Zn^{2+} storage process.[10] Moreover, proton batteries with H^+ serving as the charge carrier have demonstrated exceptional power density and cycling stability.[11] Proton hosts represent the key for efficient proton storage. To date, the reported proton hosts mainly consist of organic molecules (e.g., quinone)[12–15] and inorganic materials (e.g., MoO_3).[7,16–18] Among them, organic compounds have gained considerable attention on account of their structural diversity, ease of synthesis, and high sustainability.

Two-dimensional conjugated covalent organic frameworks (2D *c*-COFs)[19–22] represent an emerging class of layer-stacked, crystalline 2D conjugated polymers (2D CPs) with defined porosity,[23] active sites,[24] tailorable electroactivity,[25] and high charge carrier mobility,[26–29] which are promising candidates for electronic[28] and electrochemical[30–33] applications. In particular, the incorporation of redox-active units would confer unique redox behavior to the resultant 2D *c*-COFs.[34–37] Two major classes of redox-active sites, i.e. pyrazine[38] (derivatives such as phenazine, hexaazatrinaphthalene)[39] and conjugated carbonyls[40–41] (e.g., quinone,[42] naphthalene diimide[43]) have been successfully integrated into the COF backbone towards high-capacity and stable metal-ion (i.e. Zn^{2+}) storage or metal-/hydrogen-ion (i.e. Zn^{2+}/H^+) co-storage. However, pure proton storage has never been achieved among the pyrazine- or carbonyl-based COFs due to their low active-site-affinity to H^+ and relatively poor stability.[44] Therefore, exploring stable 2D *c*-COFs with strong H^+ affinity is of significance to further drive the development of proton batteries.

Herein, we report a novel poly(benzimidazobenzophenanthroline) (BBL)-ladder-type 2D *c*-COF (termed as **2DBBL-TP**) based on a new redox-active site of carbonyl dye perinone. Density functional theory (DFT) calculations indicate that the considerable π-delocalization throughout the ring-fused perinone unit contributes to a largely reduced basicity of the C–O^- groups in the reduced/discharged perinone, which leads to strong coordination ability of C–O^- to H^+ rather than Zn^{2+}. As a consequence, perinone-based **2DBBL-TP** prefers a unique proton storage behavior in both mild (aqueous $ZnCl_2$) and strong acidic (H_2SO_4) electrolytes. Remarkably, **2DBBL-TP** hybridized with carbon nanotubes (CNTs) presents an outstanding rate capability up to 200 $A\,g^{-1}$ with capacity retention of 67 % to that at 1 $A\,g^{-1}$ in H_2SO_4, which largely exceeds those of COFs and metal–organic frameworks in metal-ion storage or metal-/hydrogen-ion co-storage. Moreover, the COF electrode delivers excellent cycling stability without any detectable capacity loss after 10000 charge–discharge cycles at 100 $A\,g^{-1}$. Our work highlights the great potential of rationally designed 2D *c*-COFs in high-performance rechargeable aqueous batteries.

Results and Discussion

Design principle of active site for proton storage

To explore the competitive Zn^{2+}- and H^+-storage and design effective 2D *c*-COF for proton storage, we first performed DFT calculations to compare the molecular electronic structure, basicity/acidity, and cation binding energies of three well-known carbonyl compounds (Figure 1a). We unveil that the carbonyl dye perinone (naphthalene tetracarboxylic bisbenzimidazole, **1**) would prefer H^+- instead of Zn^{2+}-storage, while both naphthalene diimide (**2**) and pyrene-4,5,9,10-tetraone (**3**) possess a high affinity to Zn^{2+}, considering the mild aqueous Zn^{2+} electrolyte. Typically, all of them can undergo at least two-electron transfer process, where two C=O groups are reduced into C–O^- in the reduced forms (termed as **1′**, **2′** and **3′** and shown in Figure 1a). Compared to **2** and **3**, **1** exhibits extended π-conjugation and considerable intramolecular charge transfer[28]—evidenced by the electronic structures of the highest occupied molecular orbital (HOMO) and the lowest unoccupied molecular orbital (LUMO)—that contributes to a lower HOMO–LUMO gap of 2.7 eV (in comparison to 3.5 eV for **2** or **3**). The extended π-conjugation in **1** would consequently stabilize the high-energy redox intermediates[45] and decrease the basicity of the C–O^- groups in **1′** relative to **2′** and **3′**. Our hypothesis is verified by the comparison of calculated the pK_{a1} values of their conjugated acids (termed as **1″**, **2″** and **3″** and shown in Figure 1a), which predict that **1″** is more acidic than **2″** or **3″** (pK_{a1}: **1″** < **2″** < **3″**, pK_{a2} is not calculated since pK_{a1} exceeds 7). This result indicates an inferior basicity of the C–O^- groups in **1′** (referring to coordination ability to Zn^{2+}) to those in **2′** or **3′** (pK_{b1} = pK_w–pK_{a1}: **1″** > **2″** > **3″**). It is thus proposed that perinone as a redox-site could exhibit low coordination ability to Zn^{2+} and high affinity to H^+ in aqueous Zn^{2+} electrolyte.

In this context, we further calculated the binding energy of **1** towards Zn^{2+} with **2** as a reference (in the reduced forms and gas phases, see details in the Supporting Information). As expected, **1** possesses higher energies (1.64 eV) for binding one Zn^{2+} than that for **2** (1.09 eV) or other carbonyls (such as quinone[46]), suggesting a low coordination ability of perinone to Zn^{2+}. In contrast, H^+ is greatly preferred by **1** with much lower binding energies of −13.06 and −29.81 eV for one and two H^+, respectively (see the binding energies calculated in the liquid phases in Figure S1). This is in accordance with the above calculation on pK_{a1}, that is, the large π-delocalized system of perinone corresponds to decreased basicity of the C–O^- groups and subsequently enhanced affinity to specific cation (i.e. H^+). Therefore, we envision that the development of BBL-

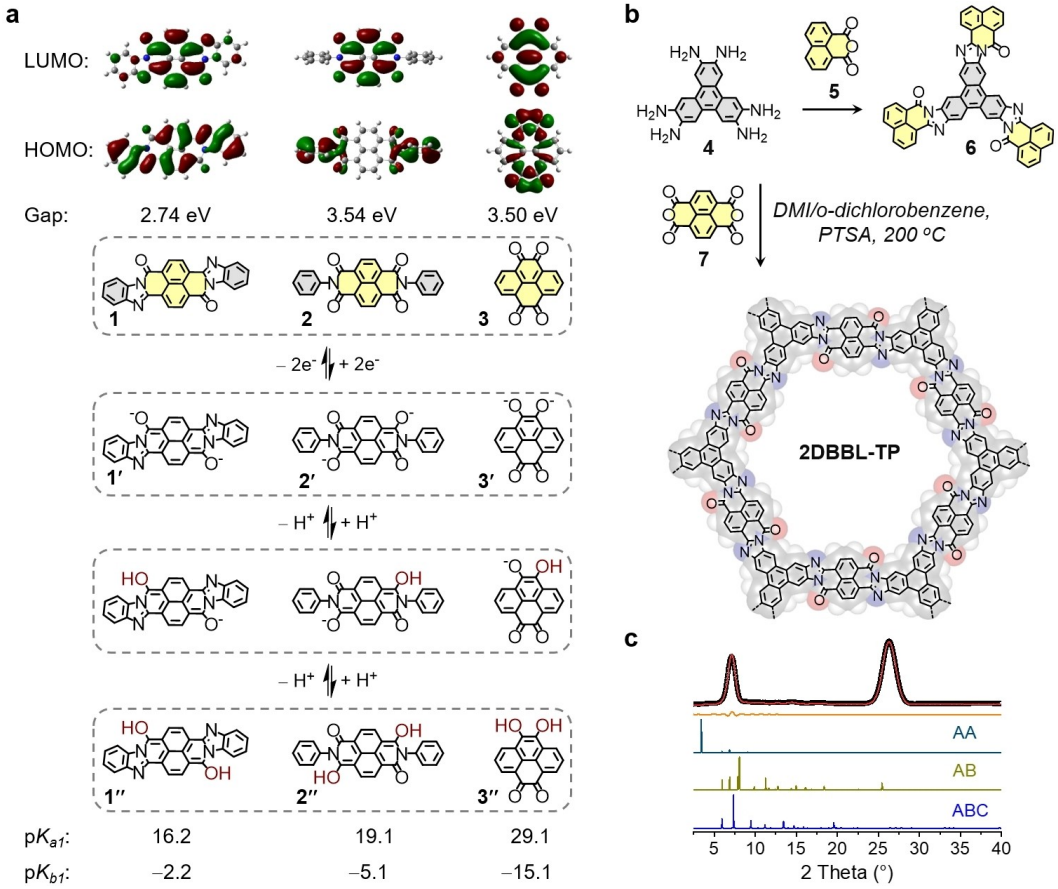

Figure 1. Design of active sites. (a) Electronic structures and proposed electron-transfer processes for model compounds **1**, **2**, and **3**. (b) Schematic synthesis of perinone-based **2DBBL-TP**. (c). Experimental (red) and refined (black) as well as the calculated PXRD patterns of **2DBBL-TP**.

ladder-type[28,47–48] 2D *c*-COF would confer good chemical stability and fast redox capability to the framework, which is promising for aqueous batteries.

Synthesis and characterization of BBL-ladder-type 2D c-COF

To examine the reactivity of a C_3-symmetric monomer—2,3,6,7,10,11-hexaaminotriphenylene (**4**)—towards BBL-ladder-type 2DCP network, we successfully synthesized model compound **6** from **4** and 1,8-naphthalic anhydride (**5**) in a 1,3-dimethyl-2-imidazolidinone/*p*-toluenesulfonic acid (DMI/PTSA) solution at 200 °C for 3 days (Figure 1b, see the ^{13}C nuclear magnetic resonance (NMR) and mass spectra of **6** in Figure 2b and Figure S2, respectively). Next, crystalline perinone-based **2DBBL-TP** was constructed through the polycondensation of **4** and naphthalenetetracarboxylic dianhydride (**7**) with PTSA as catalyst in DMI/*o*-dichlorobenzene (v/v = 2/1) at 200 °C for 5 days (Figure 1b, Table S1). Powder X-ray diffraction (PXRD) analysis reveals the crystalline nature of **2DBBL-TP** with distinct peaks at 7.28 and 26.3°, assignable to (−101) and (−104) crystallographic planes of an ABC stacking mode (Figure 1c, Figures S3 and S4). Pawley refinement provides a PXRD pattern matching well with the experimental result, as evidenced by the low R_{wp} and R_p values of 2.61 and 1.29 %, respectively (Figure S5).

The formation of imidazole rings in the perinone moiety in **2DBBL-TP** is evident by Fourier-transform infrared (FT-IR) spectroscopy displaying the appearance of C=N and C=O stretching vibration at 1660 and 1700 cm^{-1}, respectively (Figure 2a).[28,48] The peak at 1781 cm^{-1} belongs to the unreacted carbonyls at the edges. In the ^{1}H solid-state nuclear magnetic resonance (NMR) spectrum, a broad proton signal at ≈6.0 ppm appears which is attributed to aromatic protons (Figure S6). ^{13}C cross-polarization magic-angle spinning NMR spectrum shows five signals at 158.3, 148.9, 142.7, 127.9, and 107.8 ppm, which are in good agreement with the predicted spectrum (Figure 2b and Figure S7). X-ray photoelectron spectroscopy (XPS) further reveals the presence of C 1*s*, O 1*s*, and N 1*s* core levels (Figure S8). Deconvolution of the C 1*s* signal generates peaks at 284.8, 285.4 and 288.5 eV, attributable to the sp^2 C–C, C=N and C=O bond, respectively (Figure 2c, down). High-resolution N 1*s* spectrum displays peaks at 398.7 and 400.7 eV, assignable to the C–N=C and C–N–C bonds (Figure 2c, top),[28,48] which further confirms the formation of imidazole rings.

Transmission electron microscopy (TEM) imaging shows the layer-stacked 2D *c*-COF structure with an interlayer

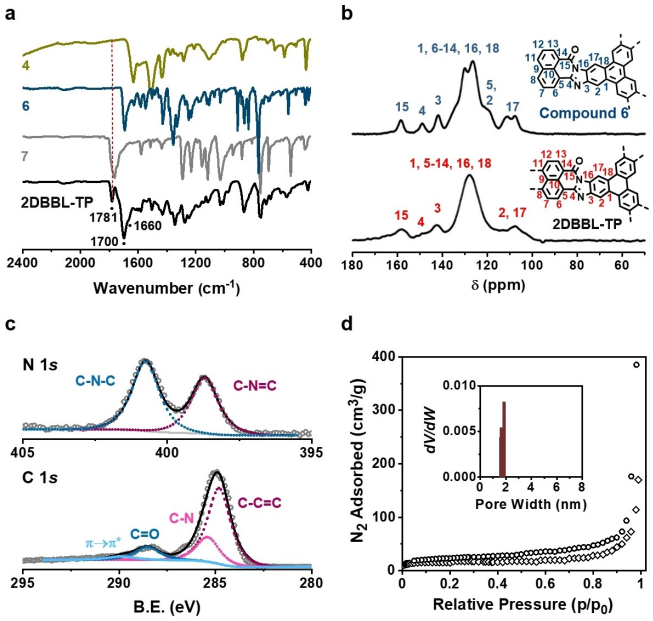

Figure 2. Characterization of **2DBBL-TP**. (a) FT-IR spectra of the starting materials, model compound **6** and **2DBBL-TP**. (b) ^{13}C NMR spectrum. The spectrum of model compound **6** is shown as a reference. (c) XPS C 1*s* and N 1*s* spectra. (d) Nitrogen physisorption and pore size distribution.

distance of ~3.5 Å (Figure S9). Field-emission scanning electron microscopy (SEM) indicates spherical aggregated particles of **2DBBL-TP** (Figure S10). Energy dispersive X-ray (EDX) spectroscopy discloses a homogeneous distribution of C, O and N elements throughout the 2D *c*-COF particles (Figure S10). The porosity was determined by low-pressure nitrogen physisorption measurements at 77 K. **2DBBL-TP** exhibits type II isotherms. The Brunauer–Emmett–Teller surface area is calculated to be 355 $m^2 g^{-1}$ (Figure 2d, the pore size distribution is shown in the inset). Thermogravimetric analysis suggests that **2DBBL-TP** is thermally stable >300 °C without significant weight loss in an argon atmosphere (Figure S11). UV/Visible-near IR spectrum of the dispersion of **2DBBL-TP** in dimethyl sulfoxide displays a broad absorption peak centered at ca. 600 nm; Tauc plot of $(Ahv)^2$ vs hv reveals its optical band gap of ~1.6 eV (Figure S12). Temperature-dependent electrical conductivity measurement depicts a semiconducting behavior of the **2DBBL-TP** pellet sample with an activation energy of 0.18 eV in the room temperature region (see details in Figure S13).

Proton storage in aqueous Zn-ion electrolyte

Taking account of the above calculated unique affinity of perinone to H^+ rather than Zn^{2+}, the robust framework of **2DBBL-TP** provides an ideal platform to investigate the redox-activity of perinone-based polymers in aqueous Zn^{2+} electrolyte. To ensure efficient charge transfer and firm interfacial contact, **2DBBL-TP** was in situ mixed with ≈25 wt % CNTs (named as **2DBBL-TP/CNTs**). As a primary attempt, we employed **2DBBL-TP/CNTs** as a cathode with Zn metal and 1 M $ZnCl_2$ aqueous solution being the counter electrode and the electrolyte, respectively (Figure S14). Figure 3a shows the typical cyclic voltammetry (CV) curve of **2DBBL-TP/CNTs** at 1 mV s^{-1} in a potential window of 0.3–1.0 V (vs Zn^{2+}/Zn). Two broad redox bands consisting of two pairs of closely overlapped peaks are observed, which indicates a two-electron transfer process for the COF.

The structural evolution of **2DBBL-TP/CNTs** was evaluated by FT-IR and XPS on the pristine, discharged and recharged electrodes. FT-IR spectra display that the C=O stretching vibration at ≈1695 cm^{-1} vanishes in the discharged electrode and reappears after recharging at 1.0 V (Figure 3b). XPS spectra suggest that the C 1*s* and N 1*s* signals are insensitive to the discharge, while positively shifted O 1*s* peak is observable in the discharged electrode (Figure 3c and Figure S15). These results disclose that C=N and C–N are not responsible for the identified redox behavior; rather only C=O functions as the active sites. Hence we propose a two-electron transfer pathway for **2DBBL-TP** as depicted in Figure 3d. In addition, multiple DFT calculations were performed on the discharged perinone to gain insights into the above electrochemical behavior (see details in Figures S16–S20).

Given that the consumption of H^+ by **2DBBL-TP** would break the original hydrolysis equilibrium of Zn^{2+} and consequently promote further hydrolysis of $Zn(OH)^+$ into $Zn(OH)_2\downarrow$ or $Zn_xCl_y(OH)_{2x-y}\downarrow$ (see details in Figure 3d and Figure S21) on the electrode surface, we examined the SEM/EDX images of the **2DBBL-TP/CNTs** electrodes. A uniform nanosheet-like deposit, which is mainly composed of Zn, O and Cl elements, was observed on the discharged electrode and completely disappeared after recharge (Figure 3e and Figures S21–S23). This result indicates the existence of $Zn_xCl_y(OH)_{2x-y}$,[49–50] associating with the proposed proton storage mechanism. Because of the same reactivity of two carbonyl groups in perinone and the absence of different plateaus in the charge–discharge curves (Figure 3f), H^+ is the predominant charge carrier of **2DBBL-TP**. Moreover, when 0.5 M zinc(II) trifluoromethanesulfonate in acetonitrile serves as the electrolyte (absence of H^+), **2DBBL-TP/CNTs** presents an entirely different electrochemical behavior with large polarization in the CV curve (Figure S24). In addition, the COF electrode delivers a limited capacity of <32 mAh g^{-1} at a much lower current density (0.1 A g^{-1}, see discussions with Figure S25 and below). These phenomena further confirm the weak affinity of **2DBBL-TP** to Zn^{2+} and the predominant proton storage mechanism of **2DBBL-TP** in aqueous Zn^{2+} electrolyte. Nevertheless, we could not exclude a trace of Zn^{2+}-storage during the discharge process. It is worth noting that carbonyl electrodes that have been previously used for pure (or predominant) proton storage usually work in strong acids, and cannot achieve coordination with H^+ in mild electrolytes (for 1 M $ZnCl_2$, $[H^+]=\approx 10^{-4}$ M, discussions shown in Figure S21). For instance, an imide-based COF comprising naphthalene diimide **2** (with similar carbonyls to **2DBBL-**

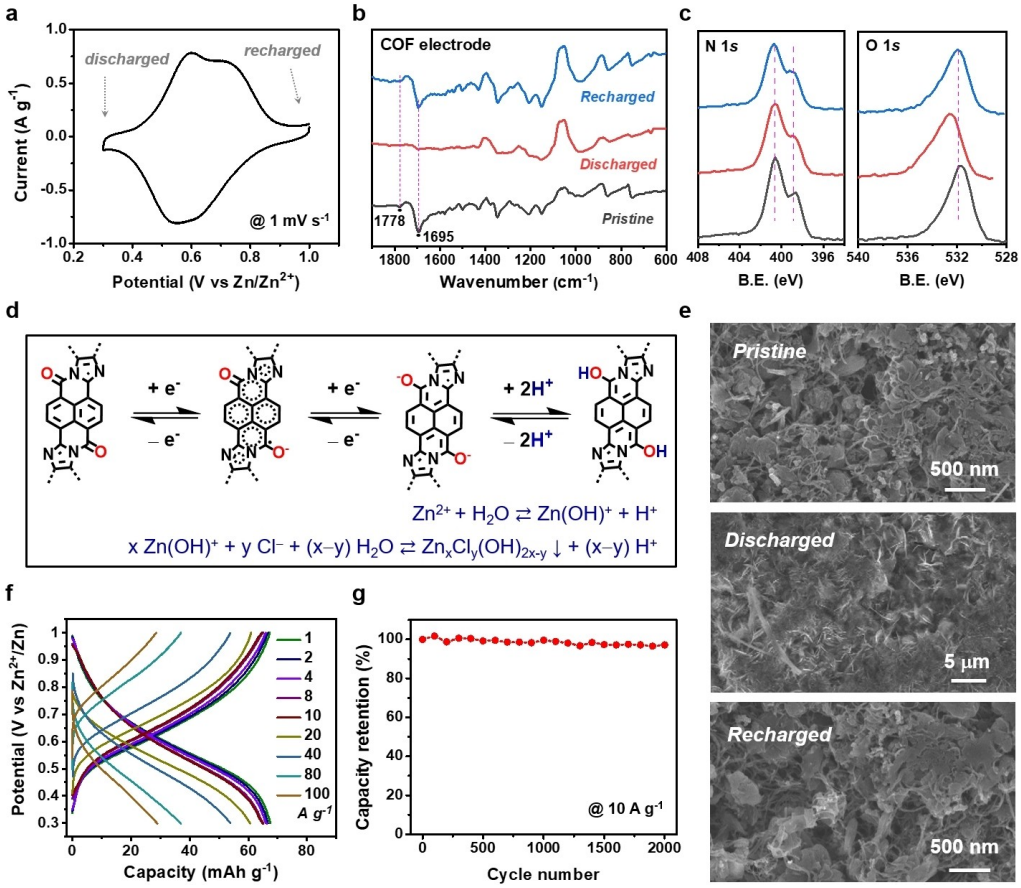

Figure 3. Proton storage of **2DBBL-TP/CNTs** in aqueous $ZnCl_2$ electrolyte. (a) CV curve. (b) FT-IR spectra. (c) XPS N 1s and O 1s spectra. (d) Proposed two-electron process during discharge. (e) SEM images of the COF electrodes. (f) Rate performance at different current densities. (g) Cycling stability.

TP) displayed a Zn^{2+}-storage mechanism in 2 M $ZnSO_4$ aqueous electrolyte.[43]

Benefiting from the fast diffusion dynamics of H^+, we further investigated the rate performance of **2DBBL-TP/CNTs** at large current densities. At 1 A g^{-1}, it delivers a stable capacity of 68 mAh g^{-1} with negligible capacity contribution from CNTs (Figure 3f and Figure S26). Increasing to 10, 20, 40 or 100 (charge period as short as ≈1 s) A g^{-1}, the COF electrode still outputs decent capacities of 65, 61, 54 or 29 mAh g^{-1}, respectively. Under accelerated scan rates (1–10 mV s^{-1}), the shape of CV curves remains nearly the same without generating much overpotential between cathodic and anodic peaks (Figure S27). Fitting the peak current response to the applied scan rate according to the power law reveals almost a pure capacitive process (Figure S28).[51–52] These results suggest that the observed charge storage in **2DBBL-TP** is pseudocapacitive in kinetics, and not dominated by solid-state ion diffusion. Furthermore, the cycling stability was evaluated at 10 A g^{-1} showing a 97.2 % capacity retention after 2000 charge–discharge cycles (Figure 3g).

Proton storage in aqueous H_2SO_4 electrolyte

The above unique proton storage behavior of **2DBBL-TP** encouraged us to investigate its electrochemical performance in strong acid. To this end, we examined the CV curve of **2DBBL-TP/CNTs** at 1 mV s^{-1} in a potential window of −0.3 to 0.3 V (vs Ag/AgCl) by using activated carbon, Ag/AgCl and 0.5 M H_2SO_4 as counter electrode, reference electrode and electrolyte, respectively. As shown in Figure 4a, two pairs of redox peaks are recorded in 0.5 M H_2SO_4 as those in 1 M $ZnCl_2$ depicted in Figure 3a. But the peaks here are clearly separated as opposed to being overlapped in the aqueous Zn^{2+} electrolyte. At 1 A g^{-1}, the COF electrode outputs a stable capacity of 76 mAh g^{-1} (Figure 4b), which is slightly higher than that achieved in 1 M $ZnCl_2$. As expected, the rate performance is evidently improved in strong acid; the capacities remain as high as 71, 69, 65 or 60 mAh g^{-1} at large current densities of 10, 20, 40 or 100 A g^{-1}, respectively. Even at 200 A g^{-1} (over 2500 C), **2DBBL-TP/CNTs** still delivers capacity up to 51 mAh g^{-1}, corresponding to capacity retention of 67 % to that at 1 A g^{-1}. It is notable that such fast reaction kinetics remarkably surpass those of metal-ion storage or metal-/hydrogen-ion co-storage among the thus-far developed

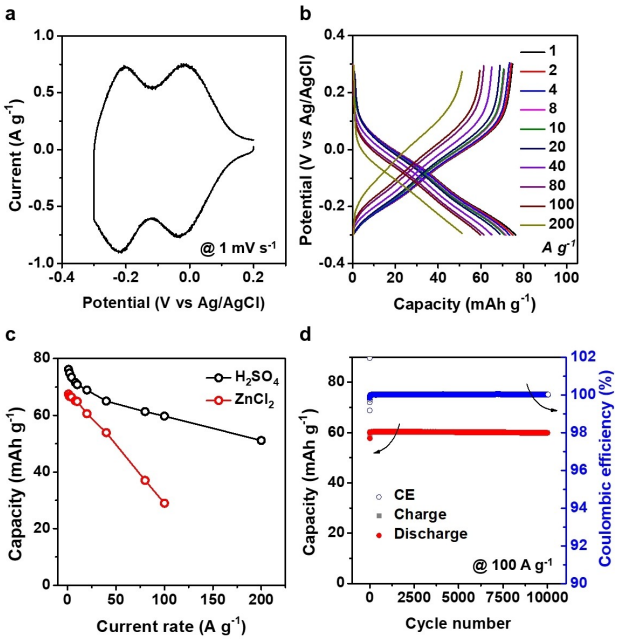

Figure 4. Electrochemical performance of **2DBBL-TP/CNTs** in aqueous H_2SO_4 electrolyte. (a) CV curve. (b) Rate performance. (c) Comparison of rate performance of **2DBBL-TP/CNTs** in 0.5 M H_2SO_4 aqueous solution with that in 1 M $ZnCl_2$. (d) Cycling stability.

rechargeable batteries (based on e.g., COFs, metal–organic frameworks, conjugated polymers, etc. see details in Figure 4c and Table S2). More importantly, **2DBBL-TP/CNTs** presents outstanding cycling stability without any perceptible capacity loss after 10000 charge–discharge cycles at 100 A g^{-1} (Figure 4d and Figure S29).

Conclusion

In summary, we have demonstrated an unprecedented preference of a BBL-ladder-type 2D *c*-COF towards proton storage in both aqueous Zn-ion electrolyte and strong acid. The BBL-ladder-type 2D *c*-COF differs from conventional carbonyl compounds and exhibits largely reduced electron density on the C–O^- groups after discharge, thus resulting in the unique proton affinity of COF electrode and an excellent rate capability up to 200 A g^{-1}. Our work highlights the great potential of developing advanced electro-/redox-active 2D *c*-COFs towards high-performance energy storage.

Acknowledgements

This work was financially supported by DFG projects (CRC 1415, No. 417590517; SPP 2248, RACOF-MMIS; GRK2861, No. 491865171), ERC Grants (T2DCP, No. 819698; FC2DMOF, No. 852909), EU Graphene Flagship (Core3, No. 881603) and Center for Advancing Electronics Dresden. R.D. thanks Taishan Scholars Program of Shandong Province (tsqn201909047), National Natural Science Foundation of China (22272092) and Natural Science Foundation of Shandong Province of China (ZR2023JQ005). G.W. acknowledges the Ningbo major Research and Development Plan Project (2023Z111). We appreciate Dresden Center for Nanoanalysis (DCN) and Dr. Petr Formanek (IPF, Dresden) for the use of facilities. We thank Dr. Yannan Liu, Dr. SangWook Park, Dr. Minghao Yu, Dr. Yanpeng Qi, Dr. Marcus Richter and Jingwei Du for helpful discussions and characterizations. Y.F. acknowledges the Center for Information Services and HPC (ZIH) at TU Dresden for the provided HPC resources. The computational resources in Mons are supported by the FNRS "Consortium des Equipements de Calcul Intensif–CECI" program Grant No. 2.5020.11. S.M.G. is Chargé de Recherche -FNRS, and D.B. is Research Director -FNRS. Open Access funding enabled and organized by Projekt DEAL.

Conflict of Interest

The authors declare no conflict of interest.

Data Availability Statement

The data that support the findings of this study are available from the corresponding author upon reasonable request.

Keywords: 2D Conjugated COFs · Poly(Benzimidazobenzophenanthroline) · Proton Storage · Strong Acid · Zn-Ion Electrolyte

[1] L. Ma, M. A. Schroeder, O. Borodin, T. P. Pollard, M. S. Ding, C. Wang, K. Xu, *Nat. Energy* **2020**, *5*, 743–749.
[2] W. Sun, F. Wang, B. Zhang, M. Zhang, V. Küpers, X. Ji, C. Theile, P. Bieker, K. Xu, C. Wang, M. Winter, *Science* **2021**, *371*, 46–51.
[3] X. Wang, C. Bommier, Z. Jian, Z. Li, R. S. Chandrabose, I. A. Rodríguez-Pérez, P. A. Greaney, X. Ji, *Angew. Chem. Int. Ed.* **2017**, *56*, 2909–2913.
[4] M. Liao, X. Ji, Y. Cao, J. Xu, X. Qiu, Y. Xie, F. Wang, C. Wang, Y. Xia, *Nat. Commun.* **2022**, *13*, 6064.
[5] L. Kong, M. Liu, H. Huang, Y. Xu, X.-H. Bu, *Adv. Energy Mater.* **2022**, *12*, 2100172.
[6] D. Zhu, G. Xu, M. Barnes, Y. Li, C.-P. Tseng, Z. Zhang, J.-J. Zhang, Y. Zhu, S. Khalil, M. M. Rahman, R. Verduzco, P. M. Ajayan, *Adv. Funct. Mater.* **2021**, *31*, 2100505.
[7] L. Zhou, L. Liu, Z. Hao, Z. Yan, X.-F. Yu, P. K. Chu, K. Zhang, J. Chen, *Matter* **2021**, *4*, 1252–1273.
[8] N. Agmon, *Chem. Phys. Lett.* **1995**, *244*, 456–462.
[9] S. Zheng, D. Shi, D. Yan, Q. Wang, T. Sun, T. Ma, L. Li, D. He, Z. Tao, J. Chen, *Angew. Chem. Int. Ed.* **2022**, *61*, e202117511.
[10] K. W. Nam, S. S. Park, R. dos Reis, V. P. Dravid, H. Kim, C. A. Mirkin, J. F. Stoddart, *Nat. Commun.* **2019**, *10*, 4948.
[11] X. Wu, J. J. Hong, W. Shin, L. Ma, T. Liu, X. Bi, Y. Yuan, Y. Qi, T. W. Surta, W. Huang, J. Neuefeind, T. Wu, P. A. Greaney, J. Lu, X. Ji, *Nat. Energy* **2019**, *4*, 123–130.
[12] F. Yue, Z. Tie, S. Deng, S. Wang, M. Yang, Z. Niu, *Angew. Chem. Int. Ed.* **2021**, *60*, 13882–13886.
[13] Z. Lin, H.-Y. Shi, L. Lin, X. Yang, W. Wu, X. Sun, *Nat. Commun.* **2021**, *12*, 4424.

[14] D. Shen, A. M. Rao, J. Zhou, B. Lu, *Angew. Chem. Int. Ed.* **2022**, *61*, e202201972.
[15] M. Yonenaga, Y. Kaiwa, K. Oka, K. Oyaizu, K. Miyatake, *Angew. Chem. Int. Ed.* **2023**, *62*, e202304366.
[16] X. Wang, Y. Xie, K. Tang, C. Wang, C. Yan, *Angew. Chem. Int. Ed.* **2018**, *57*, 11569–11573.
[17] W. Xu, K. Zhao, X. Liao, C. Sun, K. He, Y. Yuan, W. Ren, J. Li, T. Li, C. Yang, H. Cheng, Q. Sun, I. Manke, X. Lu, J. Lu, *J. Am. Chem. Soc.* **2022**, *144*, 17407–17415.
[18] Z. Ma, X.-M. Shi, S.-i. Nishimura, S. Ko, M. Okubo, A. Yamada, *Adv. Mater.* **2022**, *34*, 2203335.
[19] H. Lyu, C. S. Diercks, C. Zhu, O. M. Yaghi, *J. Am. Chem. Soc.* **2019**, *141*, 6848–6852.
[20] C. Yang, K. Jiang, Q. Zheng, X. Li, H. Mao, W. Zhong, C. Chen, B. Sun, H. Zheng, X. Zhuang, J. A. Reimer, Y. Liu, J. Zhang, *J. Am. Chem. Soc.* **2021**, *143*, 17701–17707.
[21] J. Feng, Y.-J. Zhang, S.-H. Ma, C. Yang, Z.-P. Wang, S.-Y. Ding, Y. Li, W. Wang, *J. Am. Chem. Soc.* **2022**, *144*, 6594–6603.
[22] X. Li, K. Zhang, G. Wang, Y. Yuan, G. Zhan, T. Ghosh, W. P. D. Wong, F. Chen, H.-S. Xu, U. Mirsaidov, K. Xie, J. Lin, K. P. Loh, *Nat. Synth.* **2022**, *1*, 382–392.
[23] Y. Peng, L. Li, C. Zhu, B. Chen, M. Zhao, Z. Zhang, Z. Lai, X. Zhang, C. Tan, Y. Han, Y. Zhu, H. Zhang, *J. Am. Chem. Soc.* **2020**, *142*, 13162–13169.
[24] B. P. Biswal, H. A. Vignolo-González, T. Banerjee, L. Grunenberg, G. Savasci, K. Gottschling, J. Nuss, C. Ochsenfeld, B. V. Lotsch, *J. Am. Chem. Soc.* **2019**, *141*, 11082–11092.
[25] D. Bessinger, K. Muggli, M. Beetz, F. Auras, T. Bein, *J. Am. Chem. Soc.* **2021**, *143*, 7351–7357.
[26] M. Wang, M. Ballabio, M. Wang, H.-H. Lin, B. P. Biswal, X. Han, S. Paasch, E. Brunner, P. Liu, M. Chen, M. Bonn, T. Heine, S. Zhou, E. Cánovas, R. Dong, X. Feng, *J. Am. Chem. Soc.* **2019**, *141*, 16810–16816.
[27] E. Jin, K. Geng, S. Fu, M. A. Addicoat, W. Zheng, S. Xie, J.-S. Hu, X. Hou, X. Wu, Q. Jiang, Q.-H. Xu, H. I. Wang, D. Jiang, *Angew. Chem. Int. Ed.* **2022**, *61*, e202115020.
[28] M. Wang, S. Fu, P. S. Petkov, Y. Fu, Z. Zhang, Y. Liu, J. Ma, G. Chen, S. M. Gali, L. Gao, Y. Lu, S. Paasch, H. Zhong, H.-P. Steinrück, E. Cánovas, E. Brunner, D. Beljonne, M. Bonn, H. I. Wang, R. Dong, X. Feng, *Nat. Mater.* **2023**, *22*, 880–887.
[29] Y. Liu, H. Zhang, H. Yu, Z. Liao, S. Paasch, S. Xu, R. Zhao, E. Brunner, M. Bonn, H. I. Wang, T. Heine, M. Wang, Y. Mai, X. Feng, *Angew. Chem. Int. Ed.* **2023**, *62*, e202305978.
[30] Z. Lei, Q. Yang, Y. Xu, S. Guo, W. Sun, H. Liu, L.-P. Lv, Y. Zhang, Y. Wang, *Nat. Commun.* **2018**, *9*, 576.
[31] J. Xu, Y. He, S. Bi, M. Wang, P. Yang, D. Wu, J. Wang, F. Zhang, *Angew. Chem. Int. Ed.* **2019**, *58*, 12065–12069.
[32] Y. Yue, P. Cai, K. Xu, H. Li, H. Chen, H.-C. Zhou, N. Huang, *J. Am. Chem. Soc.* **2021**, *143*, 18052–18060.
[33] X. Zhao, P. Pachfule, A. Thomas, *Chem. Soc. Rev.* **2021**, *50*, 6871–6913.
[34] X. Yang, Y. Hu, N. Dunlap, X. Wang, S. Huang, Z. Su, S. Sharma, Y. Jin, F. Huang, X. Wang, S.-h. Lee, W. Zhang, *Angew. Chem. Int. Ed.* **2020**, *59*, 20385–20389.
[35] R. Liu, K. T. Tan, Y. Gong, Y. Chen, Z. Li, S. Xie, T. He, Z. Lu, H. Yang, D. Jiang, *Chem. Soc. Rev.* **2021**, *50*, 120–242.
[36] Z. Yang, J. Liu, Y. Li, G. Zhang, G. Xing, L. Chen, *Angew. Chem. Int. Ed.* **2021**, *60*, 20754–20759.
[37] Y. Hu, L. J. Wayment, C. Haslam, X. Yang, S.-h. Lee, Y. Jin, W. Zhang, *EnergyChem* **2021**, *3*, 100048.
[38] X. Li, H. Wang, H. Chen, Q. Zheng, Q. Zhang, H. Mao, Y. Liu, S. Cai, B. Sun, C. Dun, M. P. Gordon, H. Zheng, J. A. Reimer, J. J. Urban, J. Ciston, T. Tan, E. M. Chan, J. Zhang, Y. Liu, *Chem* **2020**, *6*, 933–944.
[39] E. Vitaku, C. N. Gannett, K. L. Carpenter, L. Shen, H. D. Abruña, W. R. Dichtel, *J. Am. Chem. Soc.* **2020**, *142*, 16–20.
[40] J. Lv, Y.-X. Tan, J. Xie, R. Yang, M. Yu, S. Sun, M.-D. Li, D. Yuan, Y. Wang, *Angew. Chem. Int. Ed.* **2018**, *57*, 12716–12720.
[41] A. Khayum, M. M. Ghosh, V. Vijayakumar, A. Halder, M. Nurhuda, S. Kumar, M. Addicoat, S. Kurungot, R. Banerjee, *Chem. Sci.* **2019**, *10*, 8889–8894.
[42] H. Gao, A. R. Neale, Q. Zhu, M. Bahri, X. Wang, H. Yang, Y. Xu, R. Clowes, N. D. Browning, M. A. Little, L. J. Hardwick, A. I. Cooper, *J. Am. Chem. Soc.* **2022**, *144*, 9434–9442.
[43] M. Yu, N. Chandrasekhar, R. K. M. Raghupathy, K. H. Ly, H. Zhang, E. Dmitrieva, C. Liang, X. Lu, T. D. Kühne, H. Mirhosseini, I. M. Weidinger, X. Feng, *J. Am. Chem. Soc.* **2020**, *142*, 19570–19578.
[44] L. Cusin, H. Peng, A. Ciesielski, P. Samorì, *Angew. Chem. Int. Ed.* **2021**, *60*, 14236–14250.
[45] C. Wang, Y. Xu, Y. Fang, M. Zhou, L. Liang, S. Singh, H. Zhao, A. Schober, Y. Lei, *J. Am. Chem. Soc.* **2015**, *137*, 3124–3130.
[46] W. Wang, V. S. Kale, Z. Cao, Y. Lei, S. Kandambeth, G. Zou, Y. Zhu, E. Abouhamad, O. Shekhah, L. Cavallo, M. Eddaoudi, H. N. Alshareef, *Adv. Mater.* **2021**, *33*, 2103617.
[47] J. Wu, X. Rui, C. Wang, W.-B. Pei, R. Lau, Q. Yan, Q. Zhang, *Adv. Energy Mater.* **2015**, *5*, 1402189.
[48] H.-J. Noh, Y.-K. Im, S.-Y. Yu, J.-M. Seo, J. Mahmood, T. Yildirim, J.-B. Baek, *Nat. Commun.* **2020**, *11*, 2021.
[49] H. Pan, Y. Shao, P. Yan, Y. Cheng, K. S. Han, Z. Nie, C. Wang, J. Yang, X. Li, P. Bhattacharya, K. T. Mueller, J. Liu, *Nat. Energy* **2016**, *1*, 16039.
[50] Z. Tie, L. Liu, S. Deng, D. Zhao, Z. Niu, *Angew. Chem. Int. Ed.* **2020**, *59*, 4920–4924.
[51] V. Augustyn, J. Come, M. A. Lowe, J. W. Kim, P.-L. Taberna, S. H. Tolbert, H. D. Abruña, P. Simon, B. Dunn, *Nat. Mater.* **2013**, *12*, 518–522.
[52] G. Wang, M. Yu, J. Wang, D. Li, D. Tan, M. Löffler, X. Zhuang, K. Müllen, X. Feng, *Adv. Mater.* **2018**, *30*, 1800533.

Manuscript received: July 30, 2023
Accepted manuscript online: September 10, 2023
Version of record online: October 10, 2023